Mechanisms of Plastic Deformation in Biodegradable Polylactide/Poly(1,4-*cis*-isoprene) Blends

Marcin Kowalczyk, Ewa Piorkowska

Centre of Molecular and Macromolecular Studies, Polish Academy of Sciences, Sienkiewicza 112, 90 363 Lodz, Poland

Received 13 May 2011; accepted 20 August 2011
DOI 10.1002/app.35489
Published online 5 December 2011 in Wiley Online Library (wileyonlinelibrary.com).

ABSTRACT: Polylactide (PLA), a main representative of biodegradable and made from renewable resources polymers, is surprisingly brittle at ambient temperature. In this article it is investigated how to increase its toughness by a strategy called "rubber toughening" using poly(1,4-*cis*-isoprene), a major component of natural rubber, which is immiscible with PLA, could be well dispersed in PLA matrix and is biodegradable. Immiscible blends of PLA with poly(1,4-*cis*-isoprene) were prepared by melt blending and their properties were studied and optimized. Incorporation of as low as 5 wt % of rubber increased the strain at break of compression molded film during uniaxial drawing, and also improved its tensile impact strength by 80%. The complex mechanism of plastic deformation in the blends leading to improvement of ductility and toughness was revealed. The rubbery particles initiated crazing at the early stages of deformation, as evidenced by transmission and scanning electron microscopy and also by small angle X-ray scattering. Crazing was immediately followed by cavitation inside rubber particles, which further promoted shear yielding of PLA. The sequence of those mechanisms was proven by microscopic investigation. All three elementary mechanisms acting in the sequence indicated are responsible for surprisingly efficient toughening of PLA by a major component of natural rubber. © 2011 Wiley Periodicals, Inc. J Appl Polym Sci 124: 4579–4589, 2012

Key words: polymer blends; mechanical properties; modification

INTRODUCTION

Polylactide (PLA), a biodegradable polymer, also produced from annually renewable resources, has the glass transition temperature (T_g) in the range of 50–60°C. As a consequence, PLA is stiff and brittle at room conditions. Although both optically pure poly(L-lactide) and poly(D-lactide) are crystallizable polymers, dimers of different chirality in the polymer chain decrease its ability to crystallize without a significant change in T_g. Slowly crystallizing PLAs could be quenched below T_g without noticeable crystallization and crystallize during subsequent heating.[1,2] Crystallinity, if developed, slightly increases the modulus of elasticity and further decreases PLA's ability to plastic deformation.[3]

Significant engineering effort was made to improve PLA's mechanical properties, mostly however, without deep understanding of micromechanisms involved. To modify the mechanical properties, PLA was blended with various substances which act as plasticizers[4–10] and with other polymers.[11–21] Blending PLA with other polymers, immiscible with PLA, can lead to a substantial improvement of drawability and impact strength without a decrease in T_g. The important aspect of toughnening is retaining biodegradability of the material. The phase separated PLA-based blends with biodegradable polymers: polyhydroxyalkanoate copolymer,[11] poly(butylene adipate-*co*-terephatalate),[12] poly(ether)urethane elastomer,[13] polyamide elastomer,[14] poly(butylene succinate-*co*-lactate), and poly(butylene succinate),[15] exhibited improved ductility and toughness. Increase of the strain at break during relatively slow drawing, at the rates below 20% per minute, required incorporation of at least 10–20 wt % of the second component. Higher contents of modifiers, usually at the level of 20–40 wt %, were necessary to improve significantly the impact strength, which was accompanied by a marked decrease of the tensile strength and the elastic modulus.[12,13] Modification of PLA with polymers being neither biobased nor biodegradable, like thermoplastic polyurethane,[17] acrylonitrile-butadiene-styrene copolymer,[19] and hydrogenated styrene-butadiene-styrene block copolymer (SEBS),[20] poly(ethylene-glycidyl methacrylate) (EGMA)[21] was also examined. To control the interface, reactive blending was employed[19–21] utilizing also additional reactive components: EGMA[20,21] and styrene-acrylonitrile-glycidyl methacrylate copolymer.[19] Indeed, reactive

Correspondence to: E. Piorkowska (epiorkow@cbmm.lodz.pl).
Contract grant sponsor: European Regional Development Fund, project BioMat, 2006-2008.

blending of 70 wt % of PLA with 20 wt % of SEBS and 10 wt % of EGMA led to a material with outstanding toughness,[20] sacrificing however biodegradability.

It should be noted that dispersing nonbiodegradable polymers in biodegradable matrices leads to blends, which upon decomposition in environment will leave micrometer- or submicrometer-sized dust. Further efforts are therefore required to develop biodegradable, advantageously bio-based, modifiers for PLA. This requires better understanding of the deformation process of PLA-based blends, which is not sufficiently studied and understood.

Noda et al.[11] produced PLA/polyhydroxyalkanoate copolymer blends by melt blending, which is the usual processing method in industry. The improved toughness was a result of the molten state of fine droplets of polyhydroxyalkanoate copolymer dispersed within PLA matrix. The authors suggested that the improvement of drawability was associated with crazing because of whitening of the elongated sections of tensile specimens, which was easy to detect due to initial transparency of the blends resulted from fine dispersion and the molten state of polyhydroxyalkanoate copolymer. It has to be emphasized that in the past crazes were found in the uniaxially drawn neat glassy PLA.[8,9] Contrary to that, Jiang et al.[12] and Li and Shimizu[13] attributed the improved drawability of the PLA-based blends to debonding of the dispersed phase from PLA matrix during deformation, which facilitated shear yielding. Indeed, the debonding of the dispersed particles was evidenced by scanning electron microscopy (SEM) of the deformed specimens. However, reactive blending described by Oyama,[20] which led to supertough PLA, improved not only the dispersion of the second component but also the bonding between the particles and matrix.

It is long known that toughening of glassy polymers can be achieved by blending with another polymer, being rubbery at ambient conditions. It is recognized that multiple crazing initiated by dispersed rubber phase is one of the main mechanisms leading to an increase of toughness in systems with a glassy matrix, for instance in high impact polystyrene.[22] Other works identified void formation in rubber particles as an important part of the toughening mechanism in all rubber-modified polymers.[23,24] The conflicting reports concerning the source of toughness of PLA-based blends indicate a need for more systematic investigations of the mechanisms of plastic deformation in those systems. In this study, melt blends of linear PLA with poly(1,4-*cis*-isoprene), a major component of natural rubber, were prepared and characterized. The study was focused not only on modification of properties but also on the mechanism of plastic deformation in these blends to clarify a role of dispersed phase in the improvement of the drawability and toughness. It has to be emphasized that recently there has been considerable progress in understanding of microbial degradation of natural rubber; a possible biodegradation pathway for this abundant and technically important polymer was indicated.[25]

EXPERIMENTAL

The study utilized PLA manufactured by Hycail BV (the Netherlands), with the residual lactide content of 0.5%, according to the producer, and M_w of 125 kg mol^{-1}, $M_w/M_n = 1.3$, as determined by size-exclusion chromatography (SEC) with multi-angle laser light scattering (MALLS) detector in methylene chloride. The D-lactide and L-lactide contents were 5.25 and 94.75%, respectively, as determined by specific optical rotation measurements. Two poly(1,4-*cis*-isoprene)s purchased from Sigma Aldrich (St.Louis, MO) were used: derived from natural rubber (NR1) and synthetic (NR2). M_w and M_w/M_n determined by a SEC technique with MALLS detector in tetrahydrofuran were: 49 kg mol^{-1} and 1.9 for NR1, whereas 1380 kg mol^{-1} and 1.8 for NR2.

Prior to blending PLA was vacuum dried at 100°C for 4 h. Melt-blends containing 5, 15, and 25 wt % of rubbers were prepared using a Brabender batch mixer operating at 190°C for 20 min at 60 rpm under a flow of dry gaseous nitrogen. Neat PLA was also processed in the same manner, in order to obtain a reference material. Throughout the article the blends will be referred to as PLA/NR1 and PLA/NR2, with a number representing percentage of the rubber, for instance: PLA/NR1-5 for the blend of PLA with 5 wt % of NR1.

0.5–1 mm thick films of PLA and blends were prepared by compression molding at 180°C for 3 min, followed by quenching between thick metal blocks kept at room temperature.

All materials and molded films were then stored in a dry atmosphere in desiccators at ambient temperature.

Cryo-fracture surfaces of the films were sputtered with gold and studied under a scanning electron microscope (SEM) JEOL 5500LV (Tokyo, Japan).

Differential scanning calorimetry (DSC) was carried out with a TA Instrument 2920 DSC (New Castle, DE). Specimens of films weighing 10–12 mg were heated in the DSC at 10 °C min^{-1} under a flow of dry gaseous nitrogen.

Dynamic mechanical thermal analysis (DMTA) was carried out in a dual cantilever bending mode in a DMTA Mk III, Rheometric Scientific Ltd. apparatus (Epsom, UK), at the frequency of 1 Hz, at the heating rate of 2 °C min^{-1}, with the distance between the edge of the fixed clamp and the

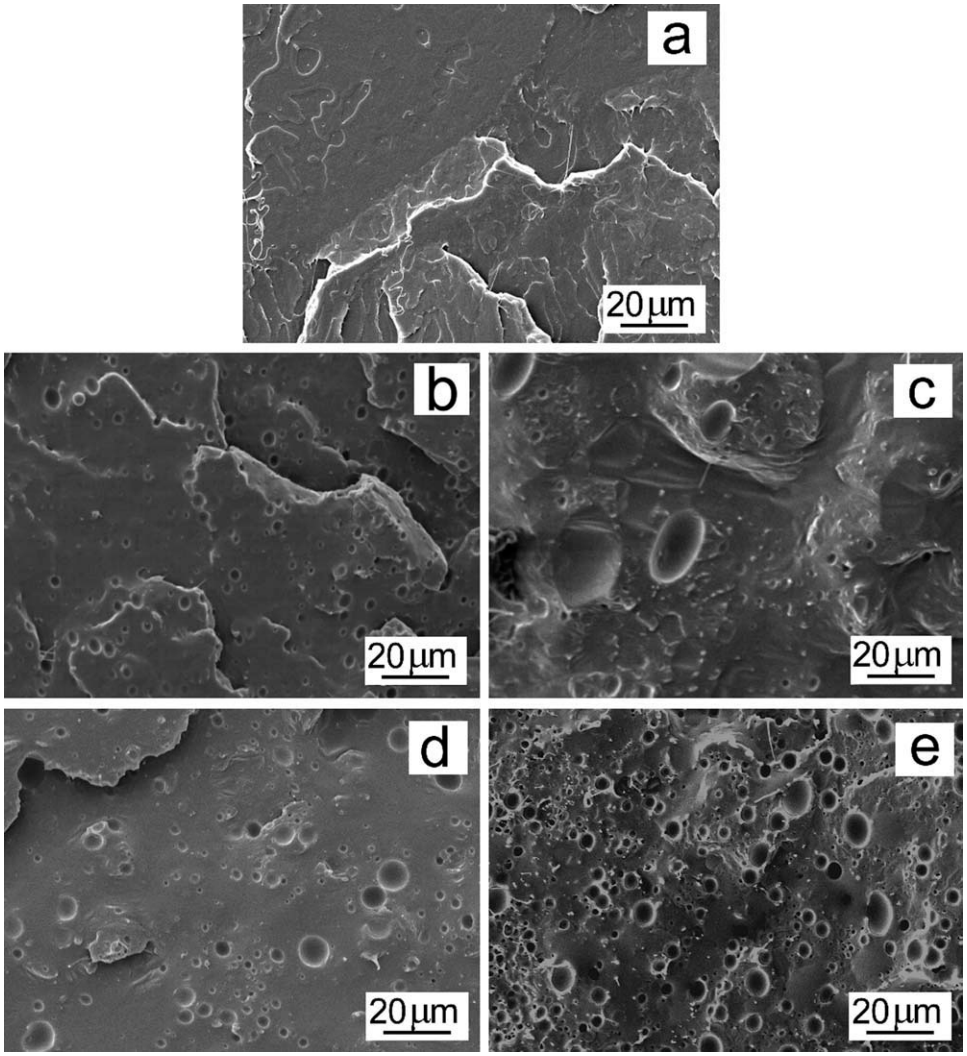

Figure 1 SEM micrographs of the surfaces of cryo-fractured samples: neat PLA (a) and blends, (b)-PLA/NR1-5, (c) PLA/NR1-15, (d) PLA/NR2-5, (e) PLA/NR2-15.

adjacent central drive clamp of 10 mm. The rectangular samples, 14 mm × 32 mm, were cut out from 1-mm thick films.

Oar-shaped specimens, conforming to ASTMD639, with the gauge length of 9.53 mm and the width of 3.18 mm, were cut out from 0.5 mm thick films for tensile tests. At least five samples of each material were drawn to fracture on an Instron (High Wycomb, UK) tensile testing machine at the rates of 0.05 min^{-1} (5% min^{-1}) and 0.5 min^{-1} (50% min^{-1}) at room temperature.

Shapes of the specimens for tensile impact tests conformed to ISO 8256: the total length of 80 mm, the narrow section length and the width of 30 and 10 mm, respectively. The specimens were cut out from 0.7 mm thick films; the thickness was adjusted to fit the absorbed energy level to the measurement range of the hammer. The tests were performed on 8–10 specimens of each of the materials using an instrumented impact tester CEAST (Charlotte, NC) Resil 5.5, with the maximum hammer energy of 1 J and velocity of 2.9 m s^{-1}.

In order to have an insight into the mechanism of deformation, specimens of selected blends were drawn to predetermined strains in the range of 0.05–2 and their structure was studied. The gauge regions of the deformed specimens were studied by DSC at the heating rate of 10 °C min^{-1} and also examined under SEM after sputtering with gold. Moreover, the gauge regions of the strained specimens, kept under stress, were studied with 2D small angle X-ray scattering (SAXS). An imaging plate (Kodak) was used as a recording medium. A 1.1-m long Kiessig-type vacuum camera was used, equipped with a capillary collimator (X-Ray Optical Systems Inc., East Greenbush, NY) enabling the resolution of scattering objects up to 40 nm. The camera was coupled to an X-ray generator (sealed-tube, fine point Cu K_α Ni filtered source, operating at 50 kV and 35 mA, Philips, Eindhoven, The Netherlands).

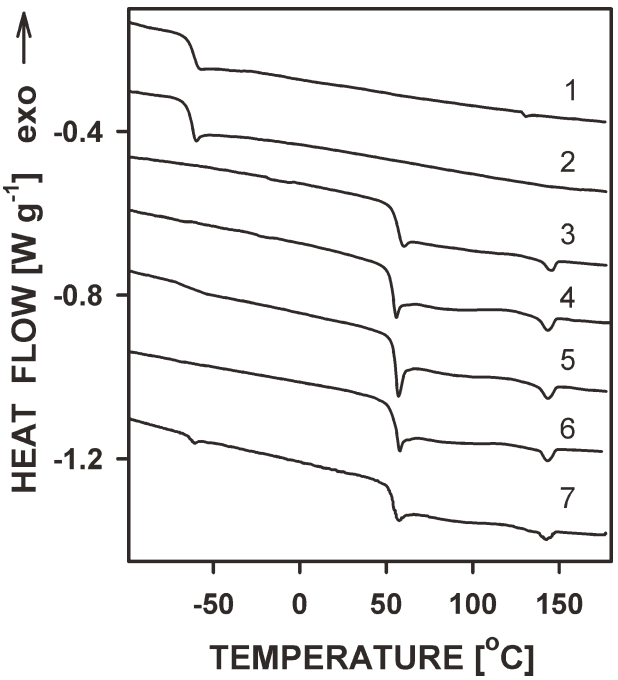

Figure 2 DSC heating thermograms of: 1—NR1 rubber, 2—NR2 rubber, 3—neat PLA and PLA blends with various rubber contents: 4—PLA/NR1-5, 5—PLA/NR1-25, 6—PLA/NR2-5, and 7—PLA/NR2-25.

Selected strained specimens were stained for 3 days with a fresh 1.5% aqueous solution of RuO_4 prepared by oxidation of $RuCl_3$ with NaOCl. 70-nm thin sections were then microtomed from the gauge regions. The ultrathin sections were cut in a plane parallel to the direction of drawing, with the cutting direction approximately at 45° to the drawing direction. The structure of the sections was studied by transmission electron microscopy (TEM) using Tesla BS 500 (Brno, the Czech Republic) operating at 90 kV. Moreover, the deformed specimens stained with RuO_4 after deformation were cryo-fractured parallel to the drawing direction. The fracture surfaces were sputtered with gold and examined under SEM.

RESULTS AND DISCUSSION

Characterization of blends

Exemplary SEM micrographs of cryo-fracture surfaces of the films of the materials prior to deformation are shown in Figure 1. The surface of PLA only bears features of brittle fracture without any heterogeneities. In contrast, the inclusions and holes left by them are clearly visible in the blends evidencing the phase separated structure. The maximum particle size in PLA/NR1 and PLA/NR2 did not exceed 10 and 18 μm, respectively. Smaller size of NR1 particles could result from lower molecular weight of NR1 and therefore higher melt viscosity ratio of the blend components. With the increase of the rubber content the maximum particle size in the blends increased to 50–60 μm.

Heating thermograms of the films are shown in Figure 2, whereas calorimetric data are collected in Table I. T_gs of all the materials were measured as the temperature corresponding to the midpoint of the heat capacity increment. The thermogram of neat PLA evidenced the glass transition with T_g at 56°C. The thermograms of NR1 and NR2 rubbers exhibited glass transitions with T_g at −62.5 and −63.5°C, respectively. All the blends showed the glass transition with T_g in the range of 54–56°C corresponding to the transition of PLA matrix. The additional low temperature glass transition was pronounced only on the thermograms of the blends with 25 wt % of rubbers; T_g values were lower by 4 and 1°C than those for neat NR1 and NR2, respectively. Such a decrease in T_g of rubber particles dispersed in a glassy polymer matrix can be a result of negative pressure, caused by different thermal contraction during cooling.[26] Neat PLA and PLA in the blends exhibited cold crystallization above the glass transition and melting as the temperature increased. The melting enthalpy, ΔH_m, equal to about 1 J g^{-1} for neat PLA and about 1–2 J g_{PLA}^{-1} for the blends, was close to the cold crystallization enthalpy, ΔH_c, in all the materials, which indicates that the samples were

TABLE I
Calorimetric Data for PLA, PLA/NR1, and PLA/NR2 Blends

Sample code	T_g (1) (°C)	T_g (2) (°C)	T_c (°C)	ΔH_c (J/g_{PLA})	T_m (°C)	ΔH_m (J/g_{PLA})
NR1	−62	–	–	–	–	–
NR2	−64	–	–	–	–	–
PLA	–	56	121	0.7	145	0.8
PLA/NR1-5	–	56	119	1.4	143	1.4
PLA/NR1-15	–	54	120	1.4	143	1.4
PLA/NR1-25	−65	56	119	1.4	143	1.6
PLA/NR2-5	–	55	119	0.8	144	1.2
PLA/NR2-15	–	55	119	1.7	144	1.8
PLA/NR2-25	−65	55	118	1.5	143	1.9

Glass transition temperature T_g, cold crystallization temperature T_c, cold crystallization enthalpy ΔH_c, melting temperature T_m, and melting enthalpy ΔH_m, measured during the first heating at the rate of 10 °C min^{-1}.

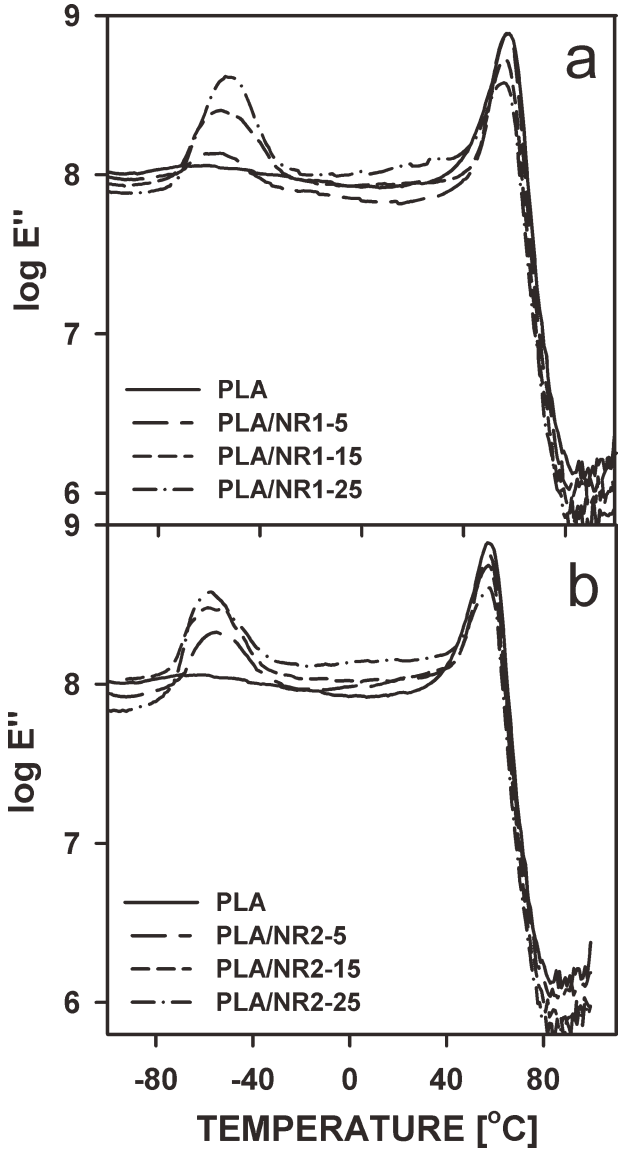

Figure 3 Temperature dependence of log E'' (in Pa) for neat PLA and blends: (a) PLA/NR1 and (b) PLA/NR2 with various rubber contents.

amorphous prior to heating in the DSC. The cold crystallization exotherms and the melting endotherms were centered at about 118–121°C and 143–145°C, respectively, and were similar for neat PLA and PLA in the blends.

TABLE II
E'' and tan δ peak Temperatures, Denoted as $T_{E''}$ and $T_{\tan\,\delta}$, respectively, for PLA and PLA Blends with NR1 and NR2 Rubbers

Sample code	$T_{E''}$ (1) (°C)	$T_{E''}$ (2) (°C)	$T_{\tan\,\delta}$ (1) (°C)	$T_{\tan\,\delta}$ (2) (°C)
PLA	–	58	–	65
PLA/NR1-5	−55	57	−55	64
PLA/NR1-15	−55	57	−53	63
PLA/NR1-25	−54	55	−52	63
PLA/NR2-5	−59	58	−55	65
PLA/NR2-15	−59	57	−55	65
PLA/NR2-25	−58	57	−55	64

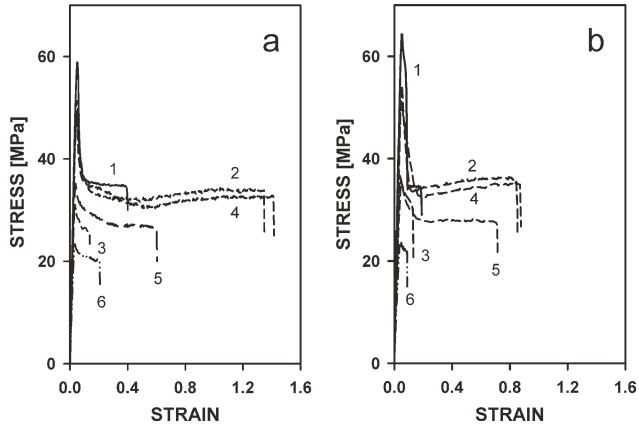

Figure 4 Stress–strain plots for: 1–neat PLA, 2—PLA/NR1-5, 3—PLA/NR1-15, 4—PLA/NR2-5, 5—PLA/NR2-15, and 6—PLA/NR2-25 blends, deformed at (a) 0.05 min^{-1} and (b) 0.5 min^{-1}.

DMTA measurements are known to be more sensitive than DSC for the detection of a second phase. Temperature dependencies of the loss modulus E'' for the materials studied are plotted in Figure 3, whereas E'' and tan δ peak temperatures are shown in Table II. The two separate E'' peaks clearly evidence two glass transitions in the blends. The low temperature peaks of PLA/NR1 and PLA/NR2 connected with glass transitions in rubbers were centered at about −55°C and −59°C, respectively, with practically no dependence on the composition of the blends. The high temperature E'' peaks of the blends, corresponding to the transition in PLA, were centered around 57–58°C, which is close to the temperature of E'' peak of neat PLA, 58°C. The only exception was PLA/NR1-25 with E'' peak at the slightly lower temperature of 55°C.

Exemplary stress–strain dependencies in tensile drawing are shown in Figure 4, whereas the mechanical data (average values) are listed in Table III. The yield stress and the stress at break diminished, whereas the strain at break increased in all the materials with a decrease in the strain rate. Independent of the strain rate, the stresses at yield and at break measured for the blends were lower than those of neat PLA. The strain at break of the blends with 5 wt % of rubbers was markedly improved in comparison to neat PLA, it increased by about 3.5 and 7 times at the strain rates of 0.05 min^{-1} and 0.5 min^{-1}, respectively. The tensile impact strength of these materials was also the highest, significantly higher than 58 kJ m^{-2} measured for neat PLA. With a further increase in the rubber content the yield stress and stress at break markedly diminished, but the strain at break and the tensile impact strength also decreased. The strains at yield were in the range of

TABLE III
Mechanical Properties of PLA, PLA/NR1, and PLA/NR2 Blends

	0.05 min^{-1}				0.5 min^{-1}				
Sample code	σ_y (MPa)	ε_y	σ_b (MPa)	ε_b	σ_y (MPa)	ε_y	σ_b (MPa)	ε_b	U (kJ m^{-2})
PLA	59.8 (1.6)	0.053 (0.002)	33.8 (1.3)	0.59 (0.46)	64.8 (1.1)	0.053 (0.003)	38.0 (2.0)	0.14 (0.09)	57.9 (6.4)
PLA/NR1-5	52.1 (0.9)	0.045 (0.002)	33.7 (1.3)	1.98 (0.71)	54.7 (1.3)	0.051 (0.002)	36.5 (0.8)	0.98 (0.39)	105.1 (9.6)
PLA/NR1-15	31.3 (0.6)	0.037 (0.003)	26.1 (1.6)	0.16 (0.07)	35.2 (0.4)	0.042 (0.002)	29.0 (2.1)	0.14 (0.07)	44.8 (5.1)
PLA/NR2-5	48.9 (1.6)	0.045 (0.002)	32.9 (1.8)	2.05 (0.77)	53.4 (1.3)	0.050 (0.004)	34.1 (1.2)	0.98 (0.40)	81.4 (9.3)
PLA/NR2-15	35.7 (0.7)	0.039 (0.001)	26.4 (1.0)	0.67 (0.37)	37.2 (0.5)	0.041 (0.002)	28.0 (0.7)	0.59 (0.33)	65.1 (6.2)
PLA/NR2-25	23.6 (0.7)	0.038 (0.002)	19.8 (0.9)	0.18 (0.09)	23.6 (1.5)	0.043 (0.005)	21.5 (0.7)	0.22 (0.09)	34.9 (4.7)

Average values of yield stress σ_y, yield strain ε_y, stress at break σ_b and strain at break ε_b, measured during uniaxial drawing at the rates of 0.05 and 0.5 min^{-1}, and tensile impact strength, U. Values of standard deviation are given in brackets.

0.038–0.054. The largest average values, 0.053–0.054, were found for neat PLA. The average yield strains for the blends with 5 wt % of rubbers were slightly smaller, 0.045 and 0.050–0.051 for the strain rates of 0.05 and 0.5 min^{-1}, respectively. An increase of the rubbers contents caused a further decrease of the yield strains.

It appears that there was no marked difference between mechanical properties of PLA/NR2-5 and PLA/NR1-5 blends, except for the tensile impact strength, which was higher for the latter.

It has to be emphasized that blending PLA with only 5 wt % of the rubbers allowed to increase strain at break and impact strength, whereas in other studies 2–4 times higher contents of biodegradable polymers were necessary to improve these properties.[12–15] As a consequence of the low content of modifier, the yield stress decreased only by 15% for PLA/NR1-5 and by 18% for PLA/NR2-5 in comparison to neat PLA.

Mechanism of plastic deformation

SEM microphotographs of the side surfaces of the tensile specimens drawn at the rate of 0.5 min^{-1}, shown in Figures 5–7, evidenced crazing at the beginning of plastic deformation. Figure 5(a) shows crazes in the PLA specimen strained to 0.05, most probably initiated by surface imperfections and impurities. Further deformation involved shear banding, as illustrated in Figure 5(b) showing a specimen strained to 0.1. As the deformation proceeded shear banding prevailed, although crazes, curved, and without sharp edges were still visible as evidenced in Figure 5(c). It has to be noted that small shear bands developing at the tips of the crazes are also shown in Figure 5(a), in a specimen strained to 0.05.

The values of strain at break of neat PLA specimens, especially those drawn at the rate of 0.05 min^{-1}, differed significantly; some of the specimens fractured at strains markedly smaller than the other. In the specimens which fractured early, only few large crazes without any shear bands were visible under SEM. Nevertheless, the values of stress at break remained similar because the glassy PLA did not exhibit any significant strain hardening. Owing to that also deviations in the strain at break of the other materials studied did not result in values of the stress at break differing significantly.

Figures 6 and 7 show SEM micrographs of the side surfaces of the gauge zones of the strained blend specimens. At the strain of 0.05, deformation was dominated by crazing, although few shear bands were also discernible, as evidenced in Figures 6(a) and 7(a). On the micrographs of the blend specimens drawn to the strain of 0.1, shown in Figures 6(b) and 7(b), pronounced shear bands surround islands with crazes similar to those shown in Figures 6(a) and 7(a). On the surface of shear bands crazes are also recognizable, but far less clearly than on the islands. Further deformation proceeded via shear banding and resulted in the structure shown in Figures 6(c) and 7(c), where at the strain of 1.0, only traces of crazes are discernible.

The presence of crazes inside the strained specimens was also evidenced by SAXS. Figure 8 shows exemplary SAXS patterns of specimens drawn at the rate of 0.5 min^{-1}, where equatorial streaks resulted from scattering on crazes. There exists a possibility that the crazes visible on the side surfaces of tensile specimens of the blends were initiated by surface imperfections or impurities. However, TEM micrograph of an ultrathin section of the interior of PLA/NR2-5 drawn to the strain of 0.1 and stained with RuO_4, shown in Figure 9, clearly evidences crazes emanating from rubbery particles embedded in PLA matrix. The same phenomenon was observed in PLA/NR1-5 blend. It must be noted that the similar results were obtained by TEM and SAXS studies for the specimens drawn at the rate of 0.05 min^{-1}. The initiation of crazes at the early stages of deformation in the blends studied undoubtedly contributed to the lowering of the yield stress in comparison to neat PLA.

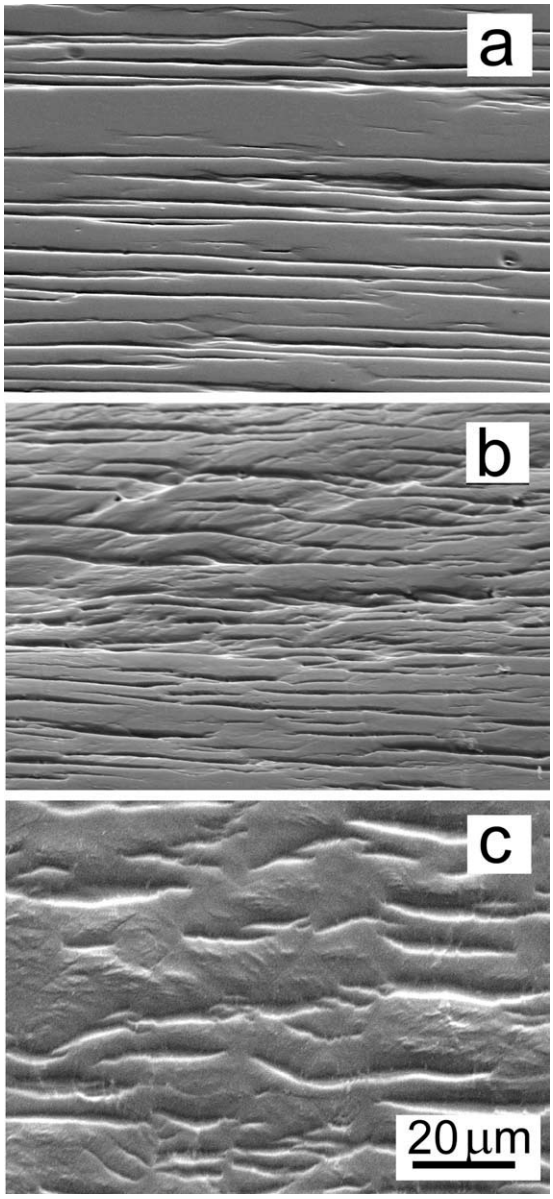

Figure 5 SEM micrographs showing the surfaces of the gauge regions of PLA specimens drawn to the strains of: (a) 0.05, (b) 0.10, and (c) 0.30. Strain rate 0.5 min^{-1}. Drawing direction—vertical.

SEM micrographs of the tensile specimens treated with RuO_4 and cryo-fractured parallel to the drawing direction are shown in Figures 10–12. Figure 10 evidences cavities inside some of the rubber particles in PLA/NR1-5 at the strain of 0.05. At the strain of 0.1 and at larger strains rows of voids were visible in the blends. In PLA/NR1-5 specimen strained to 0.1 at the rate of 0.05 min^{-1}, shown in Figure 11(a), rows of voids are inclined to the drawing direction at approx. 45°. At the top and the bottom of voids elongated in the drawing direction, remnants of rubber particles remained evidencing that cavitation occurred inside the rubber. Cavitation inside rubber particles is known to lead to the formation of cavitated shear bands. The rows of cavitated rubber particles, known as "croids", facilitate large scale shear yielding of a polymer matrix.[23,24] The increase in strain to 1.0 resulted in further elongation of voids in the drawing direction and an increase in number and size of croids, as can be seen in Figure 11(b). It can be noticed that small particles were still intact, even at the strain of 1. Figure 12 shows other specimens deformed to the strain of 1: PLA/NR1-5 drawn at the rate of 0.5 min^{-1}, and PLA/NR2-5 drawn at both rates employed. It has to be emphasized that the structure visible on the micrographs exhibits similar features as seen in Figure 11(b), independently of the material composition and the drawing rate. This points out that the mechanism of

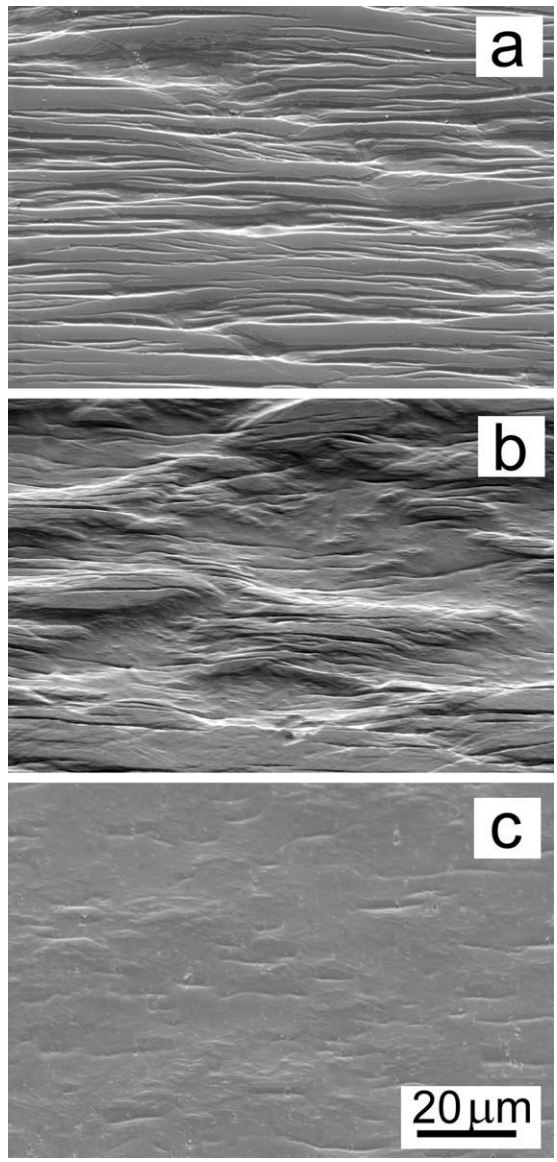

Figure 6 SEM micrographs showing the surfaces of the gauge regions of PLA/NR1-5 specimens drawn to strains of: (a) 0.05, (b) 0.10, and (c) 1.0. Strain rate 0.5 min^{-1}. Drawing direction—vertical.

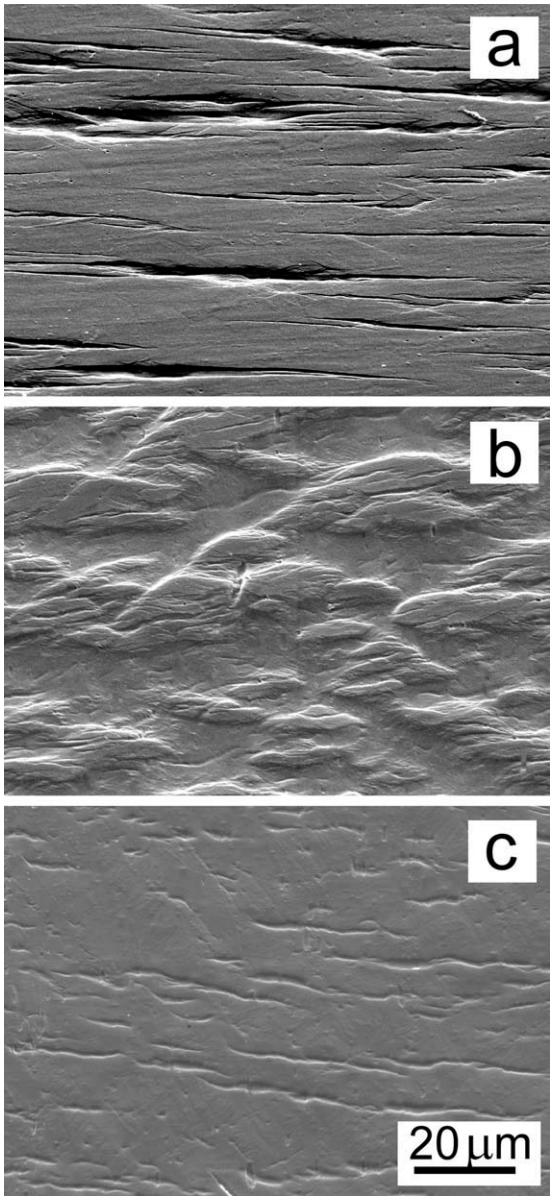

Figure 7 SEM micrographs showing the surfaces of the gauge regions of PLA/NR2-5 specimens drawn to the strains of: (a) 0.05, (b) 0.10, and (c) 1.0. Strain rate 0.5 min^{-1}. Drawing direction—vertical.

plastic deformation in the both blends was the same irrespectively of molecular weight of rubber and did not change due to an increase of the deformation rate by one order of magnitude.

It is known that the larger the rubber particles the lower the volume strain at which cavitation can occur.[23,24] Most probably, the cavitation inside large rubber particles in the blends with 15 and 25 wt % of rubbers, which occurred early, led to the formation of holes large enough to facilitate fracture at low strains.

Exemplary DSC heating thermograms of the strained specimens shown in Figure 13 evidence the glass transition of the strained specimens was

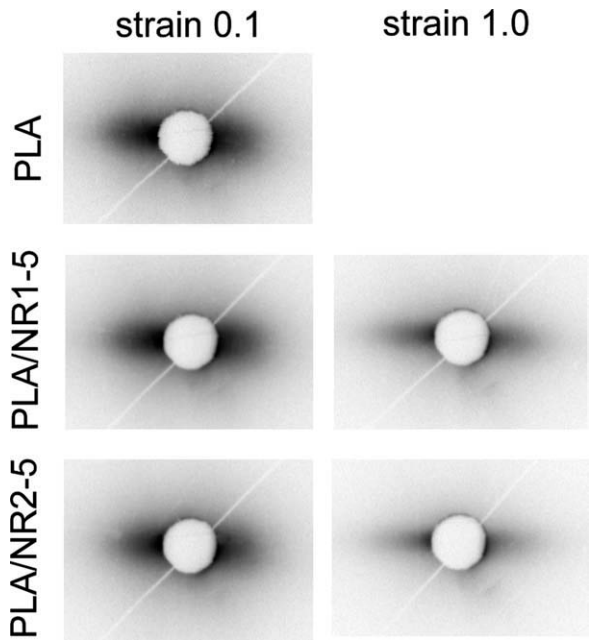

Figure 8 SAXS patterns of the gauge regions of PLA, PLA/NR1-5, and PLA/NR2-5 drawn at 0.5 min^{-1} to the strains of 0.1 and 1.0. Drawing direction—vertical.

shifted to the higher temperature and that specimens strained to 1.0 exhibited complex relaxation with a shoulder on the slope of the main peak. We hypothesize that the latter can be related to a complex deformation mechanism involving both crazing and shear bands, resulting in an inhomogeneous orientation of PLA. Above the glass transition all

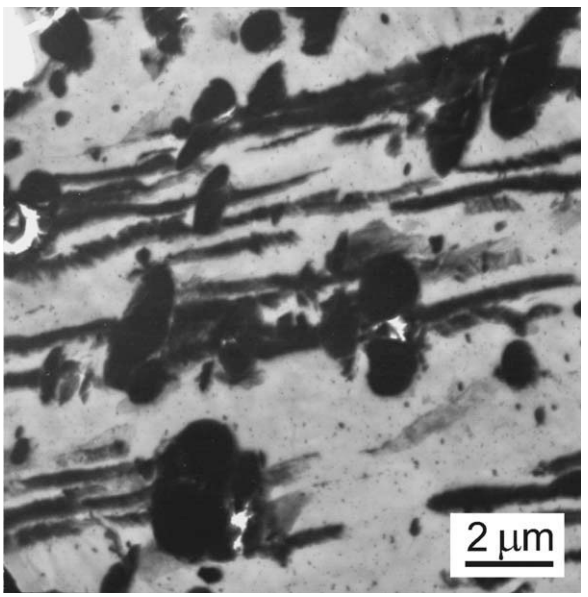

Figure 9 TEM micrograph showing an ultrathin section of the gauge region of PLA/NR2-5 specimen strained to 0.1 at the rate of 0.5 min^{-1} and treated with RuO_4. The section was cut in a plane parallel to the drawing direction, with the cutting direction approx. at 45° to the drawing direction.

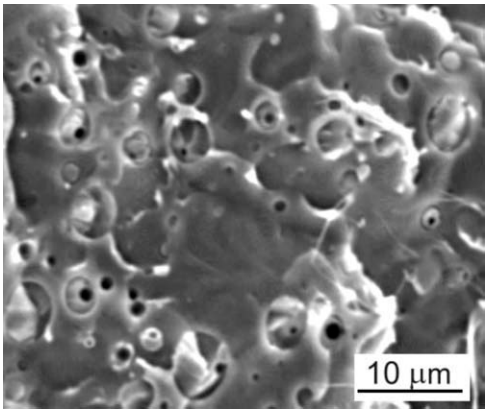

Figure 10 SEM micrograph showing the gauge region of PLA/NR1-5 specimen strained to 0.05, treated with RuO_4 for fixation and cryo-fractured along the drawing direction. Strain rate 0.5 min^{-1}. Drawing direction—vertical.

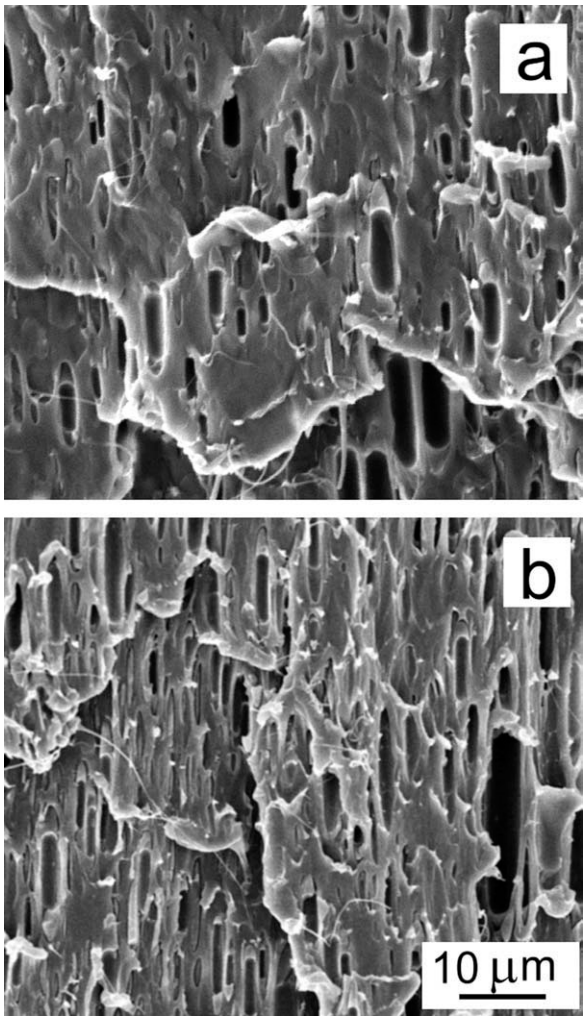

Figure 11 SEM micrographs of the gauge regions of PLA/NR1-5 specimens strained to (a) 0.1, (b) 1.0, treated with RuO_4 for fixation and cryo-fractured along the drawing direction. Strain rate 0.05 min^{-1}. Drawing direction—vertical.

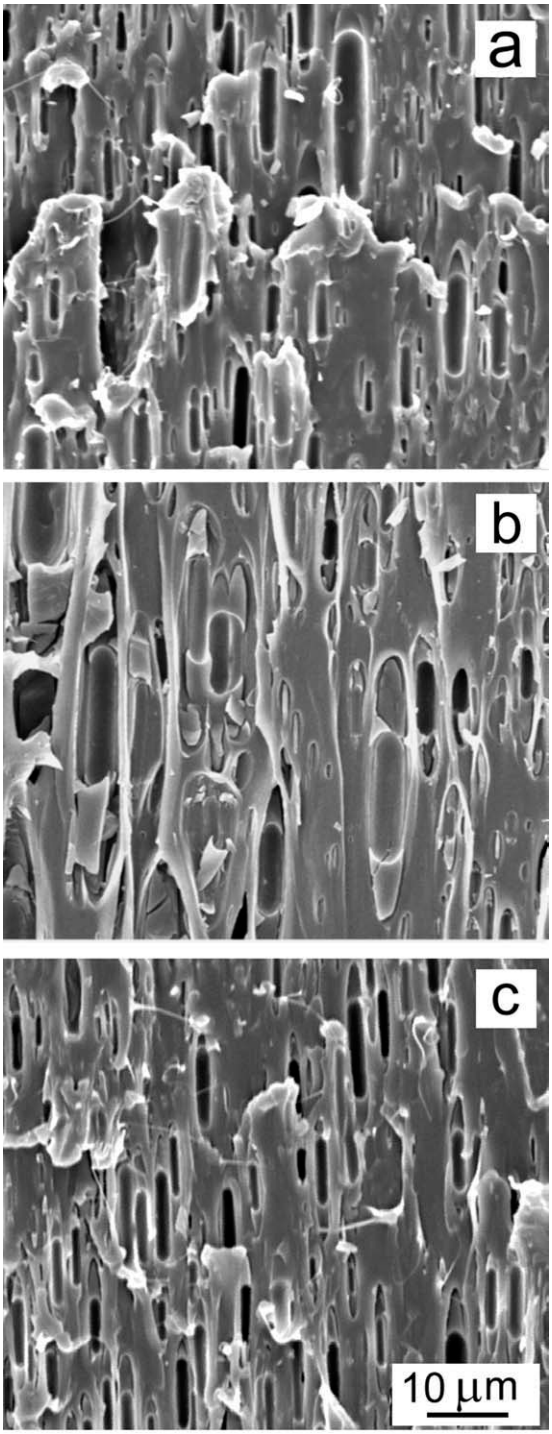

Figure 12 SEM micrographs of the gauge regions of specimens strained to 1.0, treated with RuO_4 and cryo-fractured along the drawing direction: (a) PLA/NR1-5, strain rate 0.5 min^{-1}, (b) PLA/NR2-5, strain rate 0.05 min^{-1}, (c) PLA/NR2-5, strain rate 0.5 min^{-1}. Drawing direction—vertical.

materials cold-crystallized and melted with ΔH_c and ΔH_m larger than those of undeformed materials. Moreover, ΔH_m exceeded ΔH_c indicating that PLA crystallized during drawing. $\Delta H_m - \Delta H_c$, plotted against strain in Figure 14, slightly larger for blends

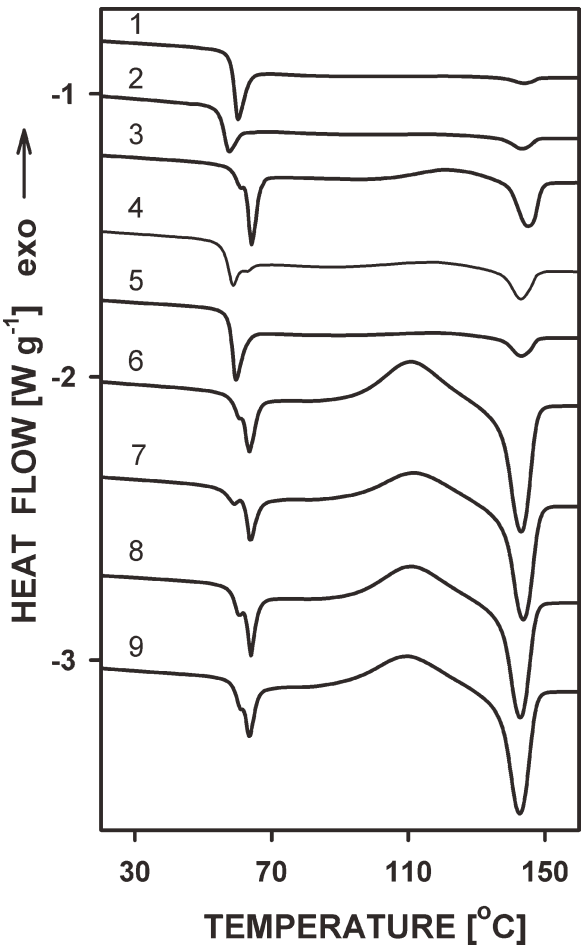

Figure 13 DSC heating thermograms of the gauge regions of strained PLA, PLA/NR1-5, and PLA/NR2-5 specimens: 1—PLA, strain 0.1, strain rate 0.05 min^{-1}, 2—PLA, strain 0.1, strain rate 0.5 min^{-1}, 3—PLA, strain 1.0, strain rate 0.05 min^{-1}, 4—PLA/NR1-5, strain 0.1, strain rate 0.05 min^{-1}, 5—PLA/NR1-5, strain 0.1, strain rate 0.5 min^{-1}, 6—PLA/NR1-5, strain 1.0, strain rate 0.05 min^{-1}, 7—PLA/NR1-5, strain 1.0, strain rate 0.5 min^{-1}, 8—PLA/NR2-5, strain 1.0, strain rate 0.05 min^{-1}, 9—PLA/NR2-5, strain 1.0, strain rate 0.5 min^{-1}.

than for neat PLA, increased with an increase in strain and reached about 2.5 J g^{-1} of PLA. This would correspond to the crystallinity level of about 2 wt %, if the enthalpy of fusion for the alpha orthorhombic form, 106 J g^{-1} was assumed.[27] We note that in other reports the strain-induced phase change in neat PLA drawn in the temperature range of 25–70°C led to the formation of the mesomorphic form.[28] The presence of strain induced phase explains the enhancement of cold crystallization in the strained materials during heating in the DSC, illustrated in Figure 13. Moreover, the effect was stronger in the blends than in neat PLA which was reflected in lower cold crystallization temperature and larger crystallization enthalpy. This is most probably related to a higher content of the strain induced phase in the deformed blend specimens, which may result from the presence of more oriented regions due to non-uniformity of deformation caused by the rubber particles.

The studies of structure of the strained specimens showed that in neat PLA plastic deformation began with crazes initiated on imperfections. However, further process was dominated by shear banding. It appears that crazes appeared first whereas shear bands developed later and formed at the tips of crazes. We note that coexisting crazes and shear bands are not usual in glassy polymers although there are cases where these modes of plastic deformation may occur simultaneously, for instance crazes and shear bands were observed in poly(ethylene terephtalate)[29] and in ethylene cycloolefin copolymer.[30] The mechanism of plastic deformation in the blends was also complex, the rubber particles played a double role, different, however, than that reported in other studies concerning PLA-based blends.[11–17] Noda et al.[11] suggested that fine droplets of polyhydroxyalkanoate copolymer toughened PLA by craze initiation. However, no other proof than whitening of strained tensile specimens visible by unarmed eye was shown. The whitening could be also caused by other phenomena, for instance cavitation inside the dispersed particles. Contrary to that, electron microscopy undoubtedly evidenced craze initiation by rubber particles in the blends studied by us, although only at the early stage of plastic deformation. With an increase in strain voiding occurred, which led to the formation of croids and facilitated shear yielding. In rubber-toughened polymers, two types of

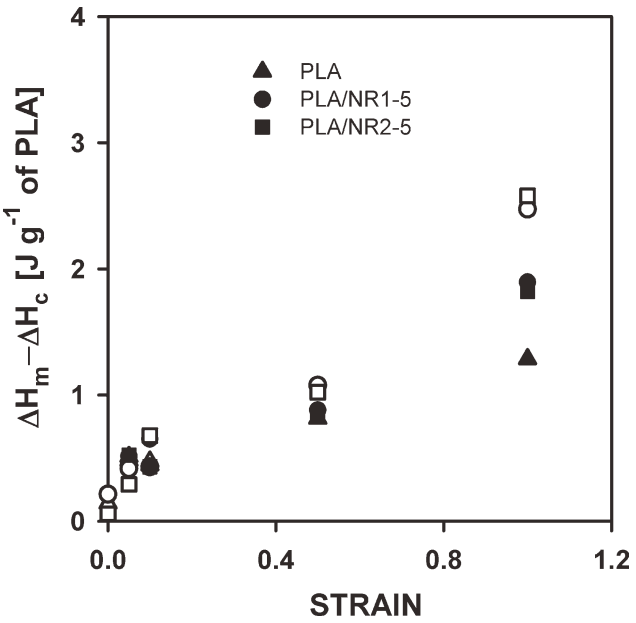

Figure 14 Dependence of $\Delta H_m - \Delta H_c$ on strain for the gauge regions of PLA, PLA/NR1-5, and PLA/NR2-5 blends. Filled symbols—strain rate 0.05 min^{-1}, empty symbols—strain rate 0.5 min^{-1}.

void formation induced by impact or tensile testing were reported: cavitation inside the rubber particles in the blends with strong interfacial adhesion, and debonding between the rubber particles and matrix when the interfacial adhesion between blend components was insufficient. In the PLA/poly(1,4-*cis*-isoprene) blends cavitation occurred inside the rubber particles, indicating a good adhesion between the components. We emphasize that although separation of the dispersed particles from PLA matrix leading to void formation was shown in Refs. [12,13], the formation of croids in PLA-based blends has not been reported so far. Moreover, the sequence of phenomena, initiation of crazes by rubbery particles followed by cavitation inside the rubber phase promoting development of shear bands, was not known before. We emphasize also that SAXS patterns evidenced crazing and that traces of crazes were observed by SEM in neat PLA and also in the blends even after a change in the deformation mechanism from crazing to shear banding. These observations can explain why, depending on a method employed in the study, either only crazing[8,9,11] or only shear yielding[12,13] in PLA and PLA-based blends were reported in the past.

CONCLUSIONS

The phase separated blends of PLA with 5 wt % of poly(1,4-*cis*-isoprene)s exhibited improved ductility and toughness in comparison to neat PLA owing to a complex mechanism of plastic deformation. The effect on tensile properties was similar for both poly(1,4-*cis*-isoprene) used, differing in molecular weight. We emphasize that the poly(1,4-*cis*-isoprene) with lower molecular weight, NR1, was derived from the natural rubber. Therefore, the entire PLA/NR1 blend can be produced from renewable resources.

The complex mechanism of plastic deformation in the blends leading to improvement of ductility and toughness was revealed. The rubbery particles initiated crazing at the early stages of deformation. Crazing was immediately followed by cavitation inside rubber particles, which further promoted shear deformation of PLA. All three elementary mechanisms acting in the sequence are responsible for surprisingly efficient toughening of PLA by blending with a small amount of poly(1,4-*cis*-isoprene)—a major component of natural rubber.

References

1. Pluta, M.; Galeski, A. J Appl Polym Sci 2002, 86, 1386.
2. Masirek, R.; Piorkowska, E.; Galeski, A.; Mucha, M. J Appl Polym Sci 2007, 105, 282.
3. Perego, G.; Cella, G. D.; Bastioli, C. J Appl Polym Sci 1996, 59, 37.
4. Labrecque, L.V.; Kumar, R. A.; Dave, V.; Gross, R. A.; McCarthy, S. P. J Appl Polym Sci 1997, 66, 1507.
5. Ljungberg, N.; Wesslen, B. J Appl Polym Sci 2002, 86, 1227.
6. Sheth, M.; Kumar, R. A.; Dave, V.; Gross, A. R.; McCarthy, S. P. J Appl Polym Sci 1997, 66, 1495.
7. Baiardo, M.; Frisoni, G.; Scandola, M.; Rimelen, M.; Lips, D.; Ruffieux, K.; Wintermantel, E. J Appl Polym Sci 2003, 90, 1731.
8. Kulinski, Z.; Piorkowska, E. Polymer 2005, 46, 10290.
9. Kulinski, Z.; Piorkowska, E.; Gadzinowska, K.; Stasiak, M. Biomacromolecules 2006, 7, 2128.
10. Piorkowska, E.; Kulinski, Z.; Galeski, A.; Masirek, R. Polymer 2006, 47, 7178.
11. Noda, I.; Satkowski, M. M.; Dowrey, A. E.; Marcott, C. Macromol Biosci 2004, 4, 269.
12. Jiang, L.; Wolcott, M. P.; Zhang, J. Biomacromolecules 2006, 7, 199.
13. Li, Y.; Shimizu, H. Macromol Biosci 2007, 7, 921.
14. Zhang, W.; Chen, L.; Zhang, Y. Polymer 2009, 50, 1311.
15. Shibata, M.; Ionue, Y.; Miyoshi, M. Polymer 2006, 47, 3557.
16. Lu, J.; Qiu, Z.; Yang, W. Polymer 2007, 48, 4196.
17. Feng, F.; Ye, L. J Appl Polym Sci 2011, 119, 2778.
18. Murariu, M.; Da Silva Ferreira, E.; Duquesne, E.; Bonnaud, L.; Dubois, Ph. Macromol Symp 2008, 272, 1.
19. Li, Y.; Shimizu, H. Eur Polym J 2009, 45, 738.
20. Hashima, K.; Nishitsuji, S.; Inoue, T. Polymer 2010, 51, 3934.
21. Oyama, H. T. Polymer 2009, 50, 747.
22. Argon, A.S.; Cohen, R. E.; Gebizlioglu, O. S.; Schwier, C. E. Adv Polym Sci 1983, 52/53, 275.
23. Lazzeri, A.; Bucknall, C. B. J Mater Sci 1993, 28, 6799.
24. Bucknall, C. B. J Polym Sci Part B: Polym Phys 2007, 45, 1399.
25. Rose, K.; Steinbuchel, A. Appl Environ Microbiol 2005, 71, 2803.
26. Bates, F. S.; Cohen, R. E.; Argon, A. S. Macromolecules 1983, 16, 1108.
27. Sarasua, J. R.; Prudhomme, R. E.; Wisniewski, M.; Le Borgne, A.; Spassky, N. Macromolecules 1998, 31, 3895.
28. Stoclet, G.; Seguela, R.; Lefebvre, J. M.; Elkoun, S.; Vanmansart, C. Macromolecules 2010, 43, 1488.
29. G'Sell, C. Revue Phys Appl 1988, 23, 1085.
30. Seydewitz, V.; Krumova, M.; Michler, G. H.; Park, J. Y., Kim, S. C. Polymer 2005, 46, 5608.